Research Article | Vol. 27, No. 4 | 18 Feb 2019 | OPTICS EXPRESS A224
Optics EXPRESS

Highly sensitive photoacoustic multicomponent gas sensor for SF_6 decomposition online monitoring

XUKUN YIN,[1,2,3] LEI DONG,[1,2,*] HONGPENG WU,[1,2] LEI ZHANG,[1,2] WEIGUANG MA,[1,2] WANGBAO YIN,[1,2] LIANTUAN XIAO,[1,2] SUOTANG JIA,[1,2] AND FRANK K. TITTEL[3]

[1]*State Key Laboratory of Quantum Optics and Quantum Optics Devices, Institute of Laser Spectroscopy, Shanxi University, Taiyuan 030006, China*
[2]*Collaborative Innovation Center of Extreme Optics, Shanxi University, Taiyuan 030006, China*
[3]*Department of Electrical and Computer Engineering, Rice University, 6100 Main Street, Houston, TX 77005, USA*
**donglei@sxu.edu.cn*

Abstract: A ppb-level photoacoustic multicomponent gas sensor system for sulfur hexafluoride (SF_6) decomposition detection was developed by the use of two near-infrared (NIR) diode lasers and an ultraviolet (UV) solid-state laser. A telecommunication fiber amplifier module was used to boost up the excitation optical power from the two NIR lasers. A dual-channel high-*Q* photoacoustic cell (PAC) was designed for the simultaneous detection of CO, H_2S, and SO_2 in SF_6 buffer gas by means of a time division multiplexing (TDM) method. Feasibility and performance of the multicomponent sensor was evaluated, resulting in minimum detection limits of 435 ppbv, 89 ppbv, and 115 ppbv for CO, H_2S, and SO_2 detection at atmospheric pressure.

1. Introduction

Sulfur hexafluoride (SF_6) was widely chosen as the preferred dielectric gas for electrical insulation or interruption purposes in electric power systems, such as in the gas-insulated switchgear, gas-insulated circuit breaker, gas-insulated transformer, transmission line and substation, due to high dielectric strength, chemically inactive and environmentally acceptable property [1,2]. Normally, pure SF_6 is colorless, odorless, nonflammable and hard to be decomposed. However, several lower fluorides of sulphur SF_x (x = 1, 2 …5) and F atoms can be generated through a corona (also called partial discharge), electric arc or spark in a gas-insulated electric power system. Although, most of the sub-fluorides will rapidly react with F atoms to regenerate SF_6 molecules again, a small portion of SF_x can further react with trace levels of unavoidable impurities (typical gases are H_2O, O_2 and N_2) or electrodes to produce numerous stable by-products [3–5]. The gaseous SF_6 decompositions (such as SO_2 and H_2S) are known to be corrosive, poisonous and chemically active, which can chemically attach the internal surface of solid insulating materials. The combination of the accumulated decomposition concentrations and the corrosive insulation materials degrade the system insulation capability, and may eventually lead to an unpredictable collapse of the electric power system. Moreover, the compositions and formation rates of SF_6 decompositions are related to the discharge insulating defect types, so that the internal status of power equipment can be identified by the composition and concentrations of SF_6 decompositions. In China, CO, H_2S and SO_2 have been recognized as indicators for the fault diagnosis of electric systems [6]. Therefore, it is critical to develop a robust, compact, and cost-effective gas sensor to monitor online the multicomponent concentration levels of SF_6 decompositions for the safety concern of personal security and electrical equipment.

#356639 https://doi.org/10.1364/OE.27.00A224
Journal © 2019 Received 7 Jan 2019; revised 25 Jan 2019; accepted 27 Jan 2019; published 13 Feb 2019

Optics EXPRESS

As a powerful diagnostic tool for the internal conditions of the gas insulated equipment, many gas analysis techniques have been developed to detect SF_6 decompositions. These detection techniques are usually divided into chemical and optical methods. Chemical methods employ adsorption, separation and different physical and chemical properties of gaseous by-products to detect the concentration levels of analytes, such as gas chromatography [7], detection nanotubes [8,9] and electrochemical sensors [10]. However, gas chromatography has a high cost, a long response time and a larger size, and is just suitable for laboratory-based investigation rather than continuous online monitoring or portable detection. Detection tubes have poor accuracy since the concentration of decomposition products is determined by color changes. Electrochemical sensors are very cheap and can be connected to the equipment to achieve online monitoring, but with zero drift and cross talk between different gases. The optical methods are based on spectral absorption technology, which offers the unique advantages of fast response time, modest cost as well as high detection selectivity and sensitivity [11–17]. Additionally, the optical-based SF_6 decomposition detection can implement online monitoring while the power system is still energized. Such an online diagnostic tool provides significant economic benefits to power plants who cannot afford to take the system out of service for accident prevention. In recent years, a variety of optical multicomponent gas sensors have been reported in N_2 or air buffer gas [18–22]. The trace gas sensors used in the SF_6 buffer gas were demonstrated but with limited success, due to the different physical and spectral characteristics of SF_6 molecules with respect to N_2, in particular the heavy molecular weight, high density as well as the unidentified absorption spectrum in the infrared (IR) spectral range [23]. For example, H. Heise *et al.* [24] and X. Zhang *et al.* [25] employed Fourier-transform infrared (FTIR) spectroscopy technology to perform quantitative multicomponent gas analysis for the SF_6 decompositions. J. Luo *et al.* [26] employed a non-resonant photoacoustic spectroscopy sensor to detect SO_2, CO and CF_4 by using a broadband light source within 4-8 μm wavelength range. However, most by-products have cross-interference absorption with pure SF_6 in the mid-infrared (MIR) region. Such a limitation results in a degraded detection accuracy and cannot meet the detection requirement of < 1 ppmv for the SF_6 gas-insulation equipment [27,28]. Therefore, it is preferable to employ an excitation source emitting at the near-infrared (NIR) or ultraviolet (UV) spectral regions and a resonant photoacoustic cell (PAC) for the optical detection technology.

In this manuscript, we reported a sensitive photoacoustic multicomponent gas sensor for the online monitoring of the SF_6 decompositions in an electric power system. The detection and quantitative measurements of trace SF_6 by-products including CO, H_2S and SO_2 were carried out via a time division multiplexing (TDM) method. A custom made two-channel differential PAC was designed with a high-*Q* factor characteristic. Two NIR telecommunication distributed feedback (DFB) lasers were used as excitation light sources emitting at 1568.1 nm and 1582.1 nm to detect CO and H_2S, respectively. A commercialized compact erbium-doped fiber amplifier (EDFA) module was employed to boost the laser powers up to 1,600 mW and 1,300mW, respectively, which compensated the absorption line-strength loss compared to the MIR spectral region. The high-power NIR laser beam was directed to one of the PAC channels, while the other channel was used to detect trace SO_2 by means of a UV-band diode-pumped solid-state laser (DPSSL). The novel combination of designed differential PAC and detection optical resources resulted in a ppb-level detection limit for the SF_6 decompositions.

2. Selection of excitation wavelengths and optical sources

According to the *HITRAN* database, SF_6 molecule has the strong v_3 band and the hot band (v_4 and $v_4 + v_6$-v_6) between 10 μm to 17.2 μm. However, the power system is filled with pure SF_6 as a dielectric gas, which means that the concentration of SF_6 is usually > 99.8%. The SF_6 absorption lines with weak line strengths cannot be ignored in the MIR spectral region,

although there are not listed in the *HITRAN* database. As shown in the upper part of Fig. 1, a SF_6 absorbance spectrum was experimentally achieved by using a FTIR spectrometer (Thermofisher Nicolet IS50) equipped with a 9.5-m multipass gas cell. The multipass gas cell was filled with pure SF_6 (>99.99%) at atmospheric pressure. Apparently, some uninterrupted SF_6 absorbance spectra were experimentally observed in the 3.3 μm - 10 μm spectral regions. The same experiments were performed, when the gas mixtures containing 50 ppmv CO, 50 ppmv H_2S and 50 ppmv SO_2 in N_2 buffer gas were fed into the gas cell. However, the experiment results showed that no absorption spectra for all the three gas mixtures were observed, since the limited detection sensitivity of the FTIR.

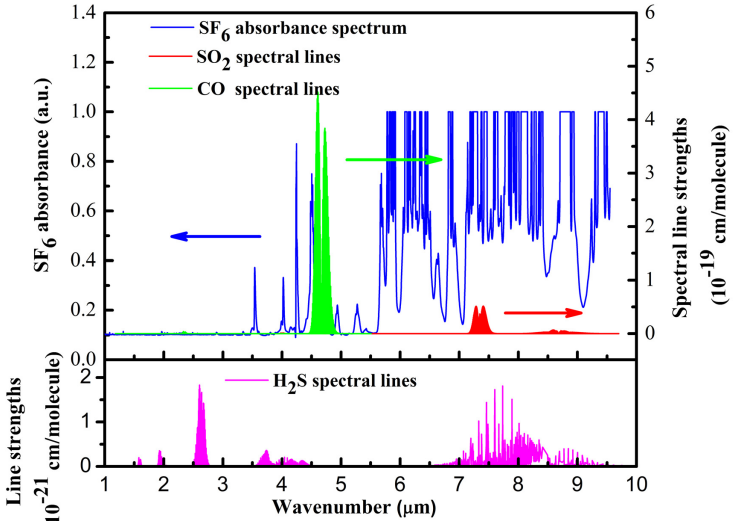

Fig. 1. Upper part: measured pure SF_6 absorbance spectra (blue line) observed by a FTIR spectrometer with a 9.5-m multipass gas cell. Simulated SO_2 (red line) and CO (green line) absorbance spectra according to the *HITRAN* database. Bottom part: simulated H_2S (magenta line) absorbance spectrum.

In order to better compare the excitation wavelengths between three target gases and SF_6, the absorption line positions and the line strengths of CO and SO_2 molecules were also plotted in the upper part of Fig. 1, according to the *HITRAN* database. The H_2S absorbance spectrum was plotted in the bottom part of Fig. 1, due to the relative weak line strengths. Obviously, the fundamental bands of CO (located around 4.7 μm) and SO_2 (around 7.3 μm) cannot be selected for the highly sensitive quantity detection of the SF_6 decompositions, owing to interfering influence with the SF_6 absorbance spectrum. The H_2S molecules showed maximum absorption line strengths near 2.7 μm and 7.8 μm between 1 μm and 10 μm spectral regions, which were about one order of magnitude lager than the overtone absorbance band around 1.6 μm. But the spectral overlap between H_2S and SF_6 occurs at 7.8 μm and the laser sources emitting at 2.7 μm have a high cost with a low output power. Furthermore, CO molecules have also an overtone absorbance band located near 1.6 μm, which cannot be observed from the upper part of Fig. 1 due to the weak line strengths. These overtone absorbance bands of H_2S and CO are located in the NIR wavelength window for fiber-optic communications. The NIR telecommunication diode lasers are competitive for trace gas detection, because of their long life (>10 years), low cost, and low power consumption [29,30]. Moreover, they can be operated at room temperature and can be fiber coupled easily to a commercial EDFA. Due to the development of the telecommunications industry, the fiber-optic amplifiers are currently able to boost the laser power up to 3~4 orders of magnitude. Thus, the amplified power compensates the weaker absorption line strengths in the overtone band. More importantly, an L-band EDFA can be used to amplify the optical

Optics EXPRESS

powers in the laser wavelength ranges from 1565 nm to 1610 nm. Such a wide wavelength range can cover several laser sources when the TDM method was used, which provides many advantages for the sensor such as a small size, low cost and portable operation.

The line selection was carefully implemented to avoid the interferences from H_2O and CO_2, since H_2O and CO_2 played an important role during the SF_6 decomposition process. As shown in Fig. 2, the molecular absorption line positions and line strengths for CO, H_2S, H_2O and CO_2 were plotted within the wavenumber range of 6319.5 cm^{-1} to 6379.0 cm^{-1}. Obviously, the two selected interference-free target absorption lines (star marks) are at least two orders of magnitude higher than the neighboring lines of the other two gases. For this work, two butterfly-type DFB lasers (Sichuan Tengguang Electronics and Technology Co., China) with central wavenumbers of 6377.4 cm^{-1} and 6320.6 cm^{-1} were selected as the excitation source to detect CO and H_2S, respectively. In order to obtain a miniaturized sensor size, a compact L-band EDFA (Connect laser technology, China) with small dimensions (20 × 13 × 5 cm^3) was utilized to amplify the excitation power up to ~1,500 mW.

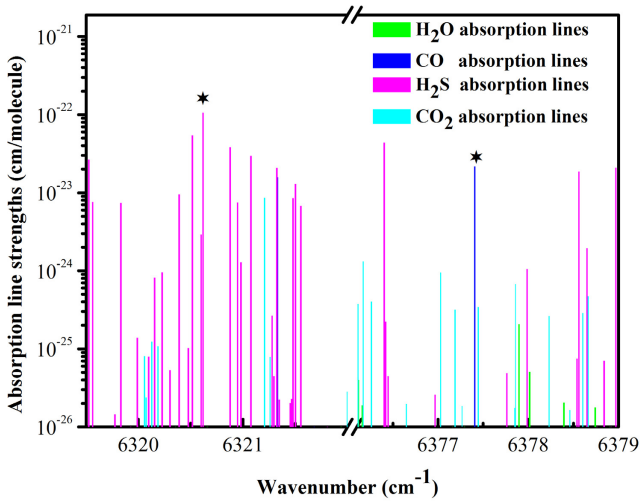

Fig. 2. Absorption line positions and line strengths of H_2O (green), H_2S (magenta), CO (blue) and CO_2 (wathet). Star marks indicate two selected interference-free target absorption lines.

According to the *HITRAN* database, there is no significant absorption for SO_2 molecules in the wavelength region between 1 μm and 3.5 μm. However, SO_2 has two strong absorption cross sections in the UV wavelength region due to electronic transitions, which provides an option for concentration measurements of SO_2. Moreover, the UV spectral region between 250 nm to 400 nm is also transparent for SF_6 molecules [6]. As shown in Fig. 3, the cross section curves of SO_2 were plotted for the second allowed band ($^1B_2 \leftarrow ^1A_1$ 165 nm-240 nm) and the first allowed band at ($^1A_2$, $^1B_1 \leftarrow ^1A_1$ 240 nm-340 nm). The maximum cross section of the second allowed band is ~36 times higher than that in the first allowed band. However, an inconspicuous absorption band of H_2S exist with a center wavelength of 195 nm, which has a cross-talk with SO_2 and hence degrades the detection limit. Therefore, the absorption band in the wavelength range of 240 nm-340 nm was chosen as the characteristic wavelengths.

Recently, a small-size and cost-effective UV laser became commercially available, due to the development of Pr^{3+}-doped based crystal lasers. It offers laser transitions in the visible spectral range, which opens a new access to the UV or even deep-UV light generation [31]. By using intra-cavity frequency doubling of a Pr:YLF-based laser and a LiB_3O_5 (LBO) crystal, a 5 mW solid-state laser emitting at 303.6 nm was achieved as the laser source to detect SO_2 in SF_6 buffer gas. The dimensions of the laser were 25 × 8 × 7 cm^3 and the spectral

linewidth is ~0.15 nm. A quality factor value of M^2 was measured to be 1.51 using a beam profiler (Thorlabs BP209-VIS/M). The dimensions of laser spot in the *x* and *y* directions were 4.5 mm and 2.5 mm at a distance of ~15 cm from the laser beam exit, respectively.

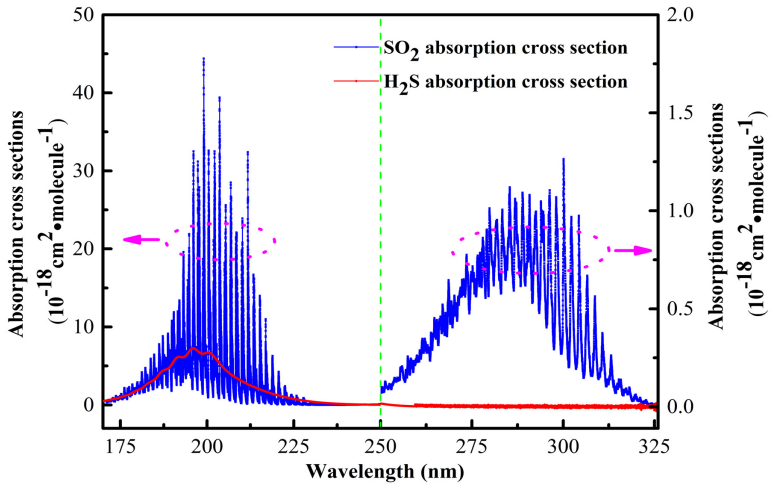

Fig. 3. SO_2 (blue line) and H_2S (red line) absorption cross section between 170 nm-325 nm.

3. Experiment setup of sensor system

3.1 Dual-channel photoacoustic detection module

The photoacoustic spectroscopy gas analysis is based on the detection of the sound signal (acoustic wave), which is generated due to localized transient heating and expansion through gas molecular collisions. The spatial size and shape of the acoustic source depend on the excitation optical beam geometry and on the absorption length in the gas. For a given excitation optical beam, the use of a PAC with high-*Q* factor is an effective way to increase the cell constant, since the photoacoustic signal is proportional to the cell constant. In general, the resonator *Q*-factor describes the energy losses during one period in the acoustic wave propagation [32,33]. For a longitudinal resonance, the contribution of the surface losses to *Q*-factor can be given as:

$$\mathrm{Q} = \frac{R}{d_{vis} + (\gamma - 1) d_{th} \left(1 + \frac{2R}{L}\right)} \tag{1}$$

where γ is the ratio of the specific heats, R and L are the radius and length of resonator, d_{vis} and d_{th} are the viscous and thermal boundary layers thicknesses. By substituting the physical constants of SF_6, a background-gas-induced high-*Q* ($Q > 50$) PAC with a dual-channel was realized for multicomponent gases detection.

As shown in Fig. 4, the stainless steel made PAC consists of two identical cylindrical resonators, each of which have a radius of 4 mm and a length of 90 mm. The inner surfaces of the resonators were polished to facilitate the formation of standing wave. In the middle of each resonator, an electret condenser cylindrical microphone (Primo, EM158) with a sensitivity of −32 dB was embedded via a 1-mm diameter hole. The two selected microphones with a dimension of Φ 6 × 10 mm have a similar response below 1.5 kHz. The signals from the two microphones were fed into a custom trans-impedance differential preamplifier with an amplification factor of 13. The gas-inlet and gas-outlet holes were

mounted in the buffer volumes, which were connected to the both ends of the resonators with a radius of 11 mm and a length of 10 mm. Two 25.4 mm × 5 mm quartz windows are used to insulate the PAC from the surrounding environment. In order to remove the light path alignment difficulty, an optical collimator (Thorlabs, F230FC-1550) is screwed onto one of the resonators in front of the entrance window, which can be used for a high power laser up to 15 W. The entrance of the other resonator is open with an 8-mm diameter through-hole for the UV laser. After passing though the resonators, both NIR and UV lasers are collected and absorbed by a black-out rough beam dump. The dual-channel photoacoustic detection module will be used for the SF_6 multicomponent decomposition analysis described in the next section.

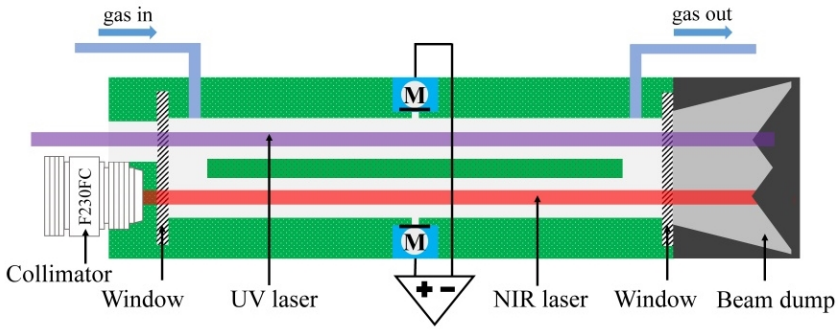

Fig. 4. Schematic of the dual-channel photoacoustic detection module.

3.2 Sensor system

A schematic of the online multicomponent gas monitoring system for the detection of the SF_6 decompositions is shown in Fig. 5. Two fiber coupled DFB lasers emitting at 1568.1 nm and 1582.1 nm were used for the detection of CO and H_2S, respectively. Wavelength modulation and second harmonic detection were employed for sensitive trace gas detection. Two 50 mHz swept ramp signals and two sine waves were generated by a digital function generator, and then added by two custom-made electric adders, respectively. The modulation frequencies of the two sine waves were set to one half of the PAC resonance frequency ($f = f_0/2$ = 343.3 Hz). The two added signals were fed into two commercial diode laser controllers (Wavelength Electronics LDTC-0520), which can sweep the laser wavelengths back and forth across the target absorption lines. The temperatures of the two DFB lasers were also controlled by the laser controllers. Both the modulated laser beams were directed to an optical switch, which can be controlled by a TTL voltage (0-5 V) for the selection of two output beams. L-band fiber amplifier module was used to boost the selected laser beam power up to 1,500 mW. The fiber amplifier module was operated in the constant power mode. An internal power meter was installed inside the fiber amplifier for a long-term output optical power calibration. After an optical collimator, a standard TEM_{00} Gaussian laser beam with a $1/e^2$ beam diameter of 0.9 mm was obtained to pass through one of the two resonators (8mm diameter). A standard square wave was generated by the function generator to modulate the solid-state laser at the resonance frequency (686.5 Hz) of the PAC. The output UV laser beam was directed at the center line of the other resonator for the detection of SO_2. A beam dump was placed behind the PAC for the collection and absorption of both the NIR and UV laser beams. The differential amplified signals from the PAC were fed into a lock-in amplifier board (FEMTO, LIA-BV-150-L), which can also be controlled by a TTL voltage signal to select the 2-*f* (CO and H_2S) or 1-*f* (SO_2) demodulation mode. Three synchronizing signals from the function generator were directed to the lock-in amplifier. A 12 dB/oct filter slope and 1 s time constant were set for the amplifier, which corresponded to a detection bandwidth of 0.25 Hz. A touch-screen computer was used for the data acquisition, logic control and signal processing via a LabVIEW routine for three target gas detection. All experiments were carried out at

atmospheric pressure and room temperature. A gas flow rate of 100 sccm was selected, which results in a gas exchange time of ~6 s between the PAC and the outside, considering a PAC volume of ~9.8 cm^3.

As shown in the inset of Fig. 5, the frequency characteristics of the PAC were experimentally investigated. At atmospheric pressure and room temperature, the fundamental longitudinal vibration frequencies of 686.5 Hz and 1772.1 Hz were achieved when filled with SF_6 and N_2 buffer gas, respectively. By calculating the ratio of resonance frequency to the half-width value of the resonance profile, a high-Q factor of 84 was obtained for SF_6 while a Q-factor of 22 was obtained for N_2, which are in excellent agreement with the calculated values of 81 and 38 for SF_6 and N_2, respectively, using Eq. (1). A detailed principle explanation for the background-gas-induced high-Q PAC can be found in our previous publication [27].

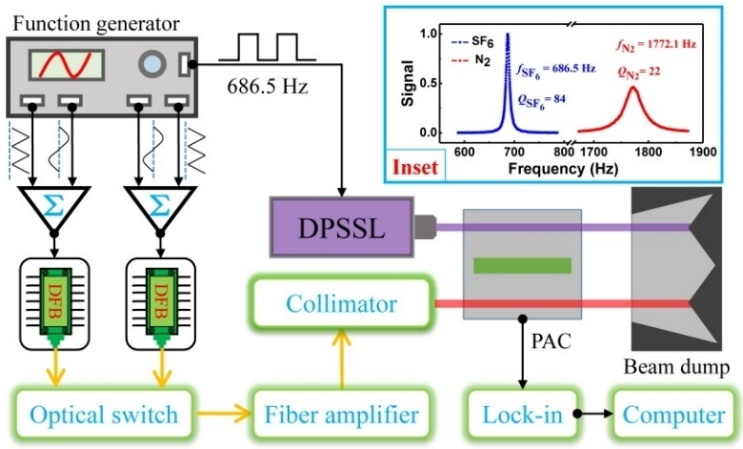

Fig. 5. Schematic of the online multicomponent gas monitoring system for SF_6 decompositions based on two NIR DFB lasers, an UV diode-pumped solid-state laser (DPSSL), a 1.5 W fiber amplifier, and a dual-channel photoacoustic cell (PAC). Inset: Resonance frequency response curves of the PAC in SF_6 (blue) and N_2 (red) buffer gases.

4. Results and discussion

The excitation power level is important for a photoacoustic gas sensor, due to the fact that the photoacoustic signal is proportional to the power. However, a saturation effect may occur with an increasing optical excitation power, so that the signal will not benefit from a higher optical power. Moreover, the erbium-doped optical fiber amplifier operating in the L-band has different power gains for different laser wavelengths. In order to achieve the gain characteristics of the selected lasers, the wavelengths of the two DFB lasers were locked at the target absorption lines (1568.1 nm and 1582.1 nm). A power meter (Ophir Optronics Solutions, 3A-ROHS) was placed behind the PAC to monitor the actual excitation power. As shown in Fig. 6(a), the actual powers of the two lasers increased linearly with the increase of the set power levels. But the laser power amplification rate was different for the two laser wavelengths. When setting the power of the fiber amplifier module to 1,500 mW, an actual power level of 1,724 mW was obtained at the wavelength of 1568.1 nm, while a power level of 1,351 mW was obtained at 1582.1 nm.

Optics EXPRESS

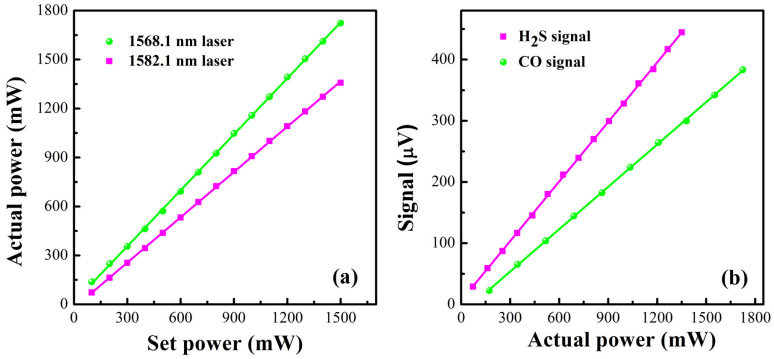

Fig. 6. (a) The actual amplified optical power levels as a function of the set power for two laser wavelengths of 1568.1 nm (green) and 1582.1 nm (magenta). (b) CO (green) and H_2S (magenta) photoacoustic signals as a function of the actual powers measured after the photoacoustic cell.

The gas mixtures containing 160 ppmv CO and 50 ppmv H_2S in SF_6 buffer gas were fed into the PAC in order to study the saturation effect. After the optimization of the modulation depths, the maximum 2-*f* signal amplitudes were recorded in Fig. 6(b). The linear fitting analysis was implemented. The obtained R-square values of 0.999 for both CO and SO_2 signals indicate that no saturation behavior with the excitation power occurred. Further experiments were implemented with the actual output mean powers of 1,724 mW and 1,351 mW for the CO and H_2S detections in order to obtain the best minimum detection limits.

In order to evaluate the detection sensitivity of the multicomponent gas sensor platform for SF_6 decompositions, the different concentrations of three target gas mixtures (CO, H_2S and SO_2) were fed into the PAC, respectively. The gas mixtures were generated by a gas dilution system (Environics EN4000). A cross-talking behaviors between three target gases was not observed due to an implementation of a good line selection. The signal data points were recorded continuously for 100 s after the signal amplitude became stable. The noise levels of the sensor were defined as the standard deviations (1σ) of the stable output signals. A 1σ standard deviation of 1.16 μV was obtained with pure SF_6 gas, which was used as the sensor noise level. As shown in Fig. 7(a), the CO/SF_6 signal amplitudes were plotted ranging from 0 ppmv to 300 ppmv. A signal amplitude of 53.4 μV with 20 ppmv CO/SF_6 gas mixtures was obtained, which resulted in a signal-to-noise ratio (SNR) of 46 and a minimum detection limit of 435 ppbv. Taking into account the laser power and the detection bandwidth, a normalized noise equivalent absorption (NNEA) coefficient of 3.8×10^{-8} $cm^{-1}WHz^{-1/2}$ was determined. As shown in Fig. 7(b), the H_2S/SF_6 signal amplitudes were plotted ranging from 0 ppmv to 8.3 ppmv. For the 1 ppmv H_2S/SF_6 gas mixtures, a detection limit of 89 ppbv and a NNEA coefficient of 2.9×10^{-8} $cm^{-1}WHz^{-1/2}$ was achieved. The SO_2/SF_6 signal amplitudes ranging from 0 ppmv to 25 ppmv were plotted in Fig. 7(c). A minimum detection limit of 115 ppbv and a NNEA coefficient of 1.8×10^{-9} $cm^{-1}WHz^{-1/2}$ were obtained with the data of 5 ppm SO_2/SF_6 gas mixtures.

Optics EXPRESS

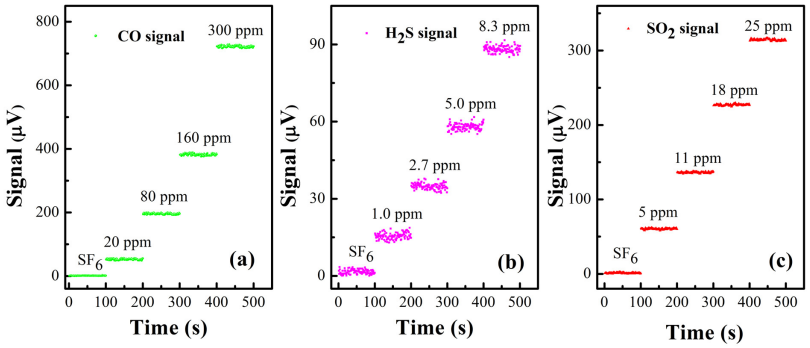

Fig. 7. (a)-(c). Photoacoustic signal amplitudes as a function of the different CO/SF_6 (green), H_2S/SF_6 (magenta) and SO_2/SF_6 (red) gas mixtures for the sensor performance evaluation.

To verify the linear concentration response, the 1000 ppmv CO/SF_6 gas was diluted with pure SF_6 to generate different concentration levels of CO/SF_6 gas mixtures. The measured maximum 2-*f* signal amplitudes as a function of the CO concentrations were plotted in Fig. 8(a). The calculated R-square value was equal to 0.9998 based on a linear fitting analysis, which indicates that the sensor system has an excellent linearity response to the CO concentration levels. The similar experiments were carried out when the 50 ppmv H_2S/SF_6 gas mixtures and the 50 ppmv SO_2/SF_6 gas mixtures were diluted with pure SF_6. As shown in Figs. 8(b) and 8(c), both the H_2S and SO_2 signals show linear responses to different concentration levels.

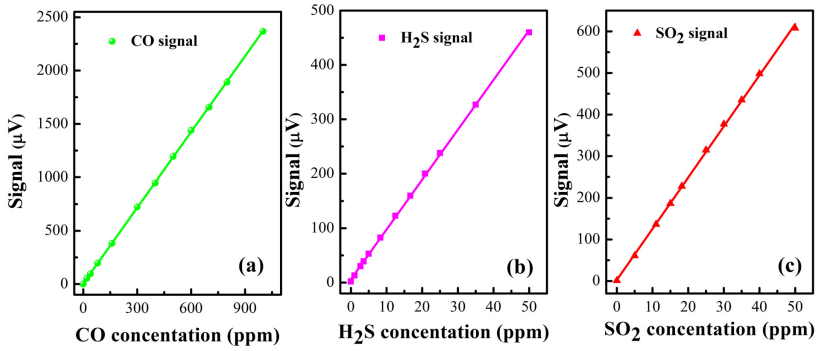

Fig. 8. (a)-(c). Response linearity of the photoacoustic Fspectroscopy-based CO (green), H_2S (magenta) and SO_2 (red) sensor system for the multicomponent SF_6 decomposition analysis.

5. Conclusion

A sensitive multicomponent gas sensor was developed for the online monitoring of SF_6 decompositions in an electric power system. By using the TDM method, a dual-channel and background-gas-induced high-*Q* PAC was designed. The selection of the excitation wavelengths and optical sources were investigated in detail, since most by-products have cross-interference absorption with SF_6 in the MIR spectral region. A commercialized L-band fiber amplifier module was used to boost the optical power of two NIR lasers for the detection of CO and H_2S, which compensated the absorption line-strength loss relative to the MIR spectral region. A novel compact DPSSL laser emitting at 303 nm was used to detect SO_2 in SF_6 buffer gas. After the optimization, the sensing capacity was validated by experimental measurements of CO, H_2S and SO_2 with the minimum detection limits of 435 ppbv, 89 ppbv and 115 ppbv, respectively. With the operating pressure of the sensor at atmospheric pressure,

an automatic gas handling system including the pressure relief for sampling and the pressurization for refilling must be employed to work together with the online multicomponent gas sensor for field applications, due to the fact that the SF_6 pressure in an electric power system is 6-8 times higher than atmospheric pressure. The optimal design of the excitation optical sources and the detection module offers a sensitive, small-size and cost-effective SF_6 decomposition sensor, which is very practical for online monitoring of an electric power system.

Funding

National Key R&D Program of China (2017YFA0304203); National Natural Science Foundation of China (NSFC) (61622503, 61575113, 61805132, 11434007); Ministry of Education of the People's Republic of China (IRT_17R70); 111 project (D18001); Sanjin Scholar (2017QNSJXZ-04); Shanxi (1331KSC); Welch Foundation (C0586); China Scholarships Council (201808140194); Outstanding Innovative Teams of Higher Learning Institutions of Shanxi; National Science Foundation (NSF) (ERC MIRTHE Award); Foundation for Selected Young Scientists Studying Abroad.

References

1. F. Y. Chu, "SF_6 decomposition in gas-insulated equipment," IEEE Trans. Electr. Insul. **EI-21**(5), 693–725 (1986).
2. X. Zhang, Y. Zhang, J. Tang, Z. Cui, Y. Li, H. Zhou, G. Zhang, and J. Yang, "Optical technology for detecting the decomposition products of SF_6: a review," Opt. Eng. **57**(11), 1 (2018).
3. V. Spagnolo, P. Patimisco, S. Borri, G. Scamarcio, B. E. Bernacki, and J. Kriesel, "Part-per-trillion level SF6 detection using a quartz enhanced photoacoustic spectroscopy-based sensor with single-mode fiber-coupled quantum cascade laser excitation," Opt. Lett. **37**(21), 4461–4463 (2012).
4. R. Cui, L. Dong, H. Wu, S. Li, L. Zhang, W. Ma, W. Yin, L. Xiao, S. Jia, and F. K. Tittel, "Highly sensitive and selective CO sensor using a 2.33 μm diode laser and wavelength modulation spectroscopy," Opt. Express **26**(19), 24318–24328 (2018).
5. M. Dong, C. Zhang, M. Ren, R. Albarracín, and R. Ye, "Electrochemical and infrared absorption spectroscopy detection of SF_6 decomposition products," Sensors (Basel) **17**(11), 2627 (2017).
6. Y. Zhang, Y. Wang, Y. Liu, X. Dong, H. Xia, Z. Zhang, and J. Li, "Optical H_2S and SO_2 sensor based on chemical conversion and partition differential optical absorption spectroscopy," Spectrochim. Acta A Mol. Biomol. Spectrosc. **210**, 120–125 (2019).
7. J. Olthoff, R. Van Brunt, J. Herron, and I. Sauers, "Detection of trace disulfur decafluoride in sulfur hexafluoride by gas chromatography/mass spectrometry," Anal. Chem. **63**(7), 726–732 (1991).
8. X. Zhang, H. Cui, Y. Gui, and J. Tang, "Mechanism and application of carbon nanotube sensors in SF_6 decomposed production detection: a review," Nanoscale Res. Lett. **12**(1), 177 (2017).
9. J. Suehiro, G. Zhou, and M. Hara, "Detection of partial discharge in SF_6 gas using a carbon nanotube-based gas sensor," Sens. Actuators B Chem. **105**(2), 164–169 (2005).
10. A. Derdouri, J. Casanovas, R. Hergli, R. Grob, and J. Mathieu, "Study of the decomposition of wet SF_6, subjected to 50-Hz ac corona discharges," J. Appl. Phys. **65**(5), 1852–1857 (1989).
11. T. Berer, M. Brandstetter, A. Hochreiner, G. Langer, W. Märzinger, P. Burgholzer, and B. Lendl, "Remote mid-infrared photoacoustic spectroscopy with a quantum cascade laser," Opt. Lett. **40**(15), 3476–3479 (2015).
12. P. Patimisco, G. Scamarcio, F. K. Tittel, and V. Spagnolo, "Quartz-enhanced photoacoustic spectroscopy: a review," Sensors (Basel) **14**(4), 6165–6206 (2014).
13. X. Yin, L. Dong, H. Wu, H. Zheng, W. Ma, L. Zhang, W. Yin, S. Jia, and F. Tittel, "Sub-ppb nitrogen dioxide detection with a large linear dynamic range by use of a differential photoacoustic cell and a 3.5 W blue multimode diode laser," Sens. Actuators B Chem. **247**, 329–335 (2017).
14. H. Yi, K. Liu, W. Chen, T. Tan, L. Wang, and X. Gao, "Application of a broadband blue laser diode to trace NO2 detection using off-beam quartz-enhanced photoacoustic spectroscopy," Opt. Lett. **36**(4), 481–483 (2011).
15. Z. Li, Z. Wang, Y. Qi, W. Jin, and W. Ren, "Improved evanescent-wave quartz-enhanced photoacoustic CO sensor using an optical fiber taper," Sens. Actuators B Chem. **248**, 1023–1028 (2017).
16. H. Zheng, M. Lou, L. Dong, H. Wu, W. Ye, X. Yin, C. S. Kim, M. Kim, W. W. Bewley, C. D. Merritt, C. L. Canedy, M. V. Warren, I. Vurgaftman, J. R. Meyer, and F. K. Tittel, "Compact photoacoustic module for methane detection incorporating interband cascade light emitting device," Opt. Express **25**(14), 16761–16770 (2017).
17. A. Foltynowicz, F. M. Schmidt, W. G. Ma, and O. Axner, "Noise-immune cavity-enhanced optical heterodyne molecular spectroscopy: Current status and future potential," Appl. Phys. B **92**(3), 313–326 (2008).
18. T. Dinh, I. Choi, Y. Son, and J. Kim, "A review on non-dispersive infrared gas sensors: improvement of sensor detection limit and interference correction," Sens. Actuators B Chem. **231**, 529–538 (2016).

Optics EXPRESS

19. H. Wu, X. Yin, L. Dong, K. Pei, A. Sampaolo, P. Patimisco, H. Zheng, W. Ma, L. Zhang, W. Yin, L. Xiao, V. Spagnolo, S. Jia, and F. Tittel, "Simultaneous dual-gas QEPAS detection based on a fundamental and overtone combined vibration of quartz tuning fork," Appl. Phys. Lett. **110**(12), 121104 (2017).
20. M. Mordmüller, M. Köhring, W. Schade, and U. Willer, "An electrically and optically cooperated QEPAS device for highly integrated gas sensors," Appl. Phys. B **119**(1), 111–118 (2015).
21. Y. Ma, R. Lewicki, M. Razeghi, and F. K. Tittel, "QEPAS based ppb-level detection of CO and N_2O using a high power CW DFB-QCL," Opt. Express **21**(1), 1008–1019 (2013).
22. M. Sigrist, R. Bartlome, D. Marinov, J. Rey, D. Vogler, and H. Wächter, "Trace gas monitoring with infrared laser-based detection schemes," Appl. Phys. B **90**(2), 289–300 (2008).
23. X. Yin, H. Wu, L. Dong, W. Ma, L. Zhang, W. Yin, L. Xiao, S. Jia, and F. Tittel, "Ppb-level photoacoustic sensor system for saturation-free CO detection of SF_6 decomposition by use of a 10 W fiber-amplified near-infrared diode laser," Sens. Actuators B Chem. **282**, 567–573 (2019).
24. H. M. Heise, R. Kurte, P. Fischer, D. Klockow, and P. R. Janissek, "Gas analysis by infrared spectroscopy as a tool for electrical fault diagnostics in SF_6 insulated equipment," Fresenius J. Anal. Chem. **358**(7–8), 793–799 (1997).
25. X. Zhang, H. Liu, J. Ren, J. Li, and X. Li, "Fourier transform infrared spectroscopy quantitative analysis of SF_6 partial discharge decomposition components," Spectrochim. Acta A Mol. Biomol. Spectrosc. **136**(Pt B), 884–889 (2015).
26. J. Luo, Y. Fang, Y. Zhao, A. Wang, D. Li, Y. Li, Y. Liu, F. Cui, J. Wu, and J. Liu, "Research on the detection of SF_6 decomposition products based on non-resonant photoacoustic spectroscopy," Anal. Methods **7**(3), 1200–1207 (2015).
27. X. Yin, L. Dong, H. Wu, W. Ma, L. Zhang, W. Yin, L. Xiao, S. Jia, and F. Tittel, "Ppb-level H_2S detection for SF_6 decomposition based on a fiber-amplified telecommunication diode laser and a background-gas-induced high-Q photoacoustic cell," Appl. Phys. Lett. **111**(3), 031109 (2017).
28. X. Yin, L. Dong, H. Wu, H. Zheng, W. Ma, L. Zhang, W. Yin, L. Xiao, S. Jia, and F. Tittel, "Highly sensitive SO_2 photoacoustic sensor for SF_6 decomposition detection using a compact mW-level diode-pumped solid-state laser emitting at 303 nm," Opt. Express **25**(26), 32581–32590 (2017).
29. Y. Ma, Y. He, X. Yu, C. Chen, R. Sun, and F. Tittel, "HCl ppb-level detection based on QEPAS sensor using a low resonance frequency quartz tuning fork," Sens. Actuators B Chem. **233**(5), 388–393 (2016).
30. X. Yin, L. Dong, H. Zheng, X. Liu, H. Wu, Y. Yang, W. Ma, L. Zhang, W. Yin, L. Xiao, and S. Jia, "Impact of humidity on quartz-enhanced photoacoustic spectroscopy based CO detection using a near-IR telecommunication diode laser," Sensors (Basel) **16**(2), 162 (2016).
31. N. Niu, S. Pu, Q. Chen, Y. Wang, Y. Zhao, W. Wu, and Q. Zheng, "302 nm continuous wave generation by intracavity frequency doubling of a diode-pumped Pr:YLF laser," Appl. Opt. **57**(33), 9798–9802 (2018).
32. A. Miklós, P. Hess, and Z. Bozóki, "Application of acoustic resonators in photoacoustic trace gas analysis and metrology," Rev. Sci. Instrum. **72**(4), 1937–1955 (2001).
33. A. Miklós, "Acoustic aspects of photoacoustic signal generation and detection in gases," Int. J. Thermophys. **36**(9), 2285–2317 (2015).